Measurement of the mass and width of the $D_{s1}(2536)^+$ meson

J. P. Lees,[1] V. Poireau,[1] E. Prencipe,[1] V. Tisserand,[1] J. Garra Tico,[2] E. Grauges,[2] M. Martinelli[ab],[3] D. A. Milanes[ab],[3] A. Palano[ab],[3] M. Pappagallo[ab],[3] G. Eigen,[4] B. Stugu,[4] L. Sun,[4] D. N. Brown,[5] L. T. Kerth,[5] Yu. G. Kolomensky,[5] G. Lynch,[5] I. L. Osipenkov,[5] H. Koch,[6] T. Schroeder,[6] D. J. Asgeirsson,[7] C. Hearty,[7] T. S. Mattison,[7] J. A. McKenna,[7] A. Khan,[8] V. E. Blinov,[9] A. R. Buzykaev,[9] V. P. Druzhinin,[9] V. B. Golubev,[9] E. A. Kravchenko,[9] A. P. Onuchin,[9] S. I. Serednyakov,[9] Yu. I. Skovpen,[9] E. P. Solodov,[9] K. Yu. Todyshev,[9] A. N. Yushkov,[9] M. Bondioli,[10] S. Curry,[10] D. Kirkby,[10] A. J. Lankford,[10] M. Mandelkern,[10] D. P. Stoker,[10] H. Atmacan,[11] J. W. Gary,[11] F. Liu,[11] O. Long,[11] G. M. Vitug,[11] C. Campagnari,[12] T. M. Hong,[12] D. Kovalskyi,[12] J. D. Richman,[12] C. A. West,[12] A. M. Eisner,[13] J. Kroseberg,[13] W. S. Lockman,[13] A. J. Martinez,[13] T. Schalk,[13] B. A. Schumm,[13] A. Seiden,[13] C. H. Cheng,[14] D. A. Doll,[14] B. Echenard,[14] K. T. Flood,[14] D. G. Hitlin,[14] P. Ongmongkolkul,[14] F. C. Porter,[14] A. Y. Rakitin,[14] R. Andreassen,[15] M. S. Dubrovin,[15] B. T. Meadows,[15] M. D. Sokoloff,[15] P. C. Bloom,[16] W. T. Ford,[16] A. Gaz,[16] M. Nagel,[16] U. Nauenberg,[16] J. G. Smith,[16] S. R. Wagner,[16] R. Ayad,[17,*] W. H. Toki,[17] H. Jasper,[18] A. Petzold,[18] B. Spaan,[18] M. J. Kobel,[19] K. R. Schubert,[19] R. Schwierz,[19] D. Bernard,[20] M. Verderi,[20] P. J. Clark,[21] S. Playfer,[21] J. E. Watson,[21] D. Bettoni[a],[22] C. Bozzi[a],[22] R. Calabrese[ab],[22] G. Cibinetto[ab],[22] E. Fioravanti[ab],[22] I. Garzia[ab],[22] E. Luppi[ab],[22] M. Munerato[ab],[22] M. Negrini[ab],[22] L. Piemontese[a],[22] R. Baldini-Ferroli,[23] A. Calcaterra,[23] R. de Sangro,[23] G. Finocchiaro,[23] M. Nicolaci,[23] S. Pacetti,[23] P. Patteri,[23] I. M. Peruzzi,[23,†] M. Piccolo,[23] M. Rama,[23] A. Zallo,[23] R. Contri[ab],[24] E. Guido[ab],[24] M. Lo Vetere[ab],[24] M. R. Monge[ab],[24] S. Passaggio[a],[24] C. Patrignani[ab],[24] E. Robutti[a],[24] B. Bhuyan,[25] V. Prasad,[25] C. L. Lee,[26] M. Morii,[26] A. J. Edwards,[27] A. Adametz,[28] J. Marks,[28] U. Uwer,[28] F. U. Bernlochner,[29] M. Ebert,[29] H. M. Lacker,[29] T. Lueck,[29] P. D. Dauncey,[30] M. Tibbetts,[30] P. K. Behera,[31] U. Mallik,[31] C. Chen,[32] J. Cochran,[32] H. B. Crawley,[32] W. T. Meyer,[32] S. Prell,[32] E. I. Rosenberg,[32] A. E. Rubin,[32] A. V. Gritsan,[33] Z. J. Guo,[33] N. Arnaud,[34] M. Davier,[34] D. Derkach,[34] J. Firmino da Costa,[34] G. Grosdidier,[34] F. Le Diberder,[34] A. M. Lutz,[34] B. Malaescu,[34] A. Perez,[34] P. Roudeau,[34] M. H. Schune,[34] A. Stocchi,[34] L. Wang,[34] G. Wormser,[34] D. J. Lange,[35] D. M. Wright,[35] I. Bingham,[36] C. A. Chavez,[36] J. P. Coleman,[36] J. R. Fry,[36] E. Gabathuler,[36] D. E. Hutchcroft,[36] D. J. Payne,[36] C. Touramanis,[36] A. J. Bevan,[37] F. Di Lodovico,[37] R. Sacco,[37] M. Sigamani,[37] G. Cowan,[38] S. Paramesvaran,[38] A. C. Wren,[38] D. N. Brown,[39] C. L. Davis,[39] A. G. Denig,[40] M. Fritsch,[40] W. Gradl,[40] A. Hafner,[40] K. E. Alwyn,[41] D. Bailey,[41] R. J. Barlow,[41] G. Jackson,[41] G. D. Lafferty,[41] R. Cenci,[42] B. Hamilton,[42] A. Jawahery,[42] D. A. Roberts,[42] G. Simi,[42] C. Dallapiccola,[43] E. Salvati,[43] R. Cowan,[44] D. Dujmic,[44] G. Sciolla,[44] D. Lindemann,[45] P. M. Patel,[45] S. H. Robertson,[45] M. Schram,[45] P. Biassoni[ab],[46] A. Lazzaro[ab],[46] V. Lombardo[a],[46] F. Palombo[ab],[46] S. Stracka[ab],[46] L. Cremaldi,[47] R. Godang,[47,‡] R. Kroeger,[47] P. Sonnek,[47] D. J. Summers,[47] X. Nguyen,[48] P. Taras,[48] G. De Nardo[ab],[49] D. Monorchio[ab],[49] G. Onorato[ab],[49] C. Sciacca[ab],[49] G. Raven,[50] H. L. Snoek,[50] C. P. Jessop,[51] K. J. Knoepfel,[51] J. M. LoSecco,[51] W. F. Wang,[51] L. A. Corwin,[52] K. Honscheid,[52] R. Kass,[52] N. L. Blount,[53] J. Brau,[53] R. Frey,[53] J. A. Kolb,[53] R. Rahmat,[53] N. B. Sinev,[53] D. Strom,[53] J. Strube,[53] E. Torrence,[53] G. Castelli[ab],[54] E. Feltresi[ab],[54] N. Gagliardi[ab],[54] M. Margoni[ab],[54] M. Morandin[a],[54] M. Posocco[a],[54] M. Rotondo[a],[54] F. Simonetto[ab],[54] R. Stroili[ab],[54] E. Ben-Haim,[55] M. Bomben,[55] G. R. Bonneaud,[55] H. Briand,[55] G. Calderini,[55] J. Chauveau,[55] O. Hamon,[55] Ph. Leruste,[55] G. Marchiori,[55] J. Ocariz,[55] S. Sitt,[55] M. Biasini[ab],[56] E. Manoni[ab],[56] A. Rossi[ab],[56] C. Angelini[ab],[57] G. Batignani[ab],[57] S. Bettarini[ab],[57] M. Carpinelli[ab],[57,§] G. Casarosa[ab],[57] A. Cervelli[ab],[57] F. Forti[ab],[57] M. A. Giorgi[ab],[57] A. Lusiani[ac],[57] N. Neri[ab],[57] E. Paoloni[ab],[57] G. Rizzo[ab],[57] J. J. Walsh[a],[57] D. Lopes Pegna,[58] C. Lu,[58] J. Olsen,[58] A. J. S. Smith,[58] A. V. Telnov,[58] F. Anulli[a],[59] G. Cavoto[a],[59] R. Faccini[ab],[59] F. Ferrarotto[a],[59] F. Ferroni[ab],[59] M. Gaspero[ab],[59] L. Li Gioi[a],[59] M. A. Mazzoni[a],[59] G. Piredda[a],[59] C. Buenger,[60] T. Hartmann,[60] T. Leddig,[60] H. Schröder,[60] R. Waldi,[60] T. Adye,[61] E. O. Olaiya,[61] F. F. Wilson,[61] S. Emery,[62] G. Hamel de Monchenault,[62] G. Vasseur,[62] Ch. Yèche,[62] M. T. Allen,[63] D. Aston,[63] D. J. Bard,[63] R. Bartoldus,[63] J. F. Benitez,[63] C. Cartaro,[63] M. R. Convery,[63] J. Dorfan,[63] G. P. Dubois-Felsmann,[63] W. Dunwoodie,[63] R. C. Field,[63] M. Franco Sevilla,[63] B. G. Fulsom,[63] A. M. Gabareen,[63] M. T. Graham,[63] P. Grenier,[63] C. Hast,[63] W. R. Innes,[63] M. H. Kelsey,[63] H. Kim,[63] P. Kim,[63] M. L. Kocian,[63] D. W. G. S. Leith,[63] P. Lewis,[63] S. Li,[63] B. Lindquist,[63] S. Luitz,[63] V. Luth,[63] H. L. Lynch,[63] D. B. MacFarlane,[63] D. R. Muller,[63] H. Neal,[63] S. Nelson,[63] C. P. O'Grady,[63] I. Ofte,[63] M. Perl,[63] T. Pulliam,[63] B. N. Ratcliff,[63] S. H. Robertson,[63] A. Roodman,[63] A. A. Salnikov,[63] V. Santoro,[63] R. H. Schindler,[63] J. Schwiening,[63] A. Snyder,[63] D. Su,[63] M. K. Sullivan,[63] S. Sun,[63] K. Suzuki,[63] J. M. Thompson,[63] J. Va'vra,[63] A. P. Wagner,[63] M. Weaver,[63] W. J. Wisniewski,[63] M. Wittgen,[63] D. H. Wright,[63] H. W. Wulsin,[63] A. K. Yarritu,[63] C. C. Young,[63] V. Ziegler,[63] X. R. Chen,[64] W. Park,[64] M. V. Purohit,[64] R. M. White,[64] J. R. Wilson,[64] A. Randle-Conde,[65] S. J. Sekula,[65] M. Bellis,[66] P. R. Burchat,[66] T. S. Miyashita,[66] M. S. Alam,[67] J. A. Ernst,[67] N. Guttman,[68] A. Soffer,[68] P. Lund,[69] S. M. Spanier,[69] R. Eckmann,[70] J. L. Ritchie,[70] A. M. Ruland,[70] C. J. Schilling,[70]

Work supported in part by US Department of Energy contract DE-AC02-76SF00515.

SLAC National Accelerator Laboratory, Menlo Park, CA 94025

R. F. Schwitters,[70] B. C. Wray,[70] J. M. Izen,[71] X. C. Lou,[71] F. Bianchi[ab],[72] D. Gamba[ab],[72] M. Pelliccioni[ab],[72] L. Lanceri[ab],[73] L. Vitale[ab],[73] N. Lopez-March,[74] F. Martinez-Vidal,[74] A. Oyanguren,[74] H. Ahmed,[75] J. Albert,[75] Sw. Banerjee,[75] H. H. F. Choi,[75] K. Hamano,[75] G. J. King,[75] R. Kowalewski,[75] M. J. Lewczuk,[75] C. Lindsay,[75] I. M. Nugent,[75] J. M. Roney,[75] R. J. Sobie,[75] T. J. Gershon,[76] P. F. Harrison,[76] T. E. Latham,[76] E. M. T. Puccio,[76] H. R. Band,[77] S. Dasu,[77] Y. Pan,[77] R. Prepost,[77] C. O. Vuosalo,[77] and S. L. Wu[77]

(The *BABAR* Collaboration)

[1]*Laboratoire d'Annecy-le-Vieux de Physique des Particules (LAPP), Université de Savoie, CNRS/IN2P3, F-74941 Annecy-Le-Vieux, France*
[2]*Universitat de Barcelona, Facultat de Fisica, Departament ECM, E-08028 Barcelona, Spain*
[3]*INFN Sezione di Bari[a]; Dipartimento di Fisica, Università di Bari[b], I-70126 Bari, Italy*
[4]*University of Bergen, Institute of Physics, N-5007 Bergen, Norway*
[5]*Lawrence Berkeley National Laboratory and University of California, Berkeley, California 94720, USA*
[6]*Ruhr Universität Bochum, Institut für Experimentalphysik 1, D-44780 Bochum, Germany*
[7]*University of British Columbia, Vancouver, British Columbia, Canada V6T 1Z1*
[8]*Brunel University, Uxbridge, Middlesex UB8 3PH, United Kingdom*
[9]*Budker Institute of Nuclear Physics, Novosibirsk 630090, Russia*
[10]*University of California at Irvine, Irvine, California 92697, USA*
[11]*University of California at Riverside, Riverside, California 92521, USA*
[12]*University of California at Santa Barbara, Santa Barbara, California 93106, USA*
[13]*University of California at Santa Cruz, Institute for Particle Physics, Santa Cruz, California 95064, USA*
[14]*California Institute of Technology, Pasadena, California 91125, USA*
[15]*University of Cincinnati, Cincinnati, Ohio 45221, USA*
[16]*University of Colorado, Boulder, Colorado 80309, USA*
[17]*Colorado State University, Fort Collins, Colorado 80523, USA*
[18]*Technische Universität Dortmund, Fakultät Physik, D-44221 Dortmund, Germany*
[19]*Technische Universität Dresden, Institut für Kern- und Teilchenphysik, D-01062 Dresden, Germany*
[20]*Laboratoire Leprince-Ringuet, CNRS/IN2P3, Ecole Polytechnique, F-91128 Palaiseau, France*
[21]*University of Edinburgh, Edinburgh EH9 3JZ, United Kingdom*
[22]*INFN Sezione di Ferrara[a]; Dipartimento di Fisica, Università di Ferrara[b], I-44100 Ferrara, Italy*
[23]*INFN Laboratori Nazionali di Frascati, I-00044 Frascati, Italy*
[24]*INFN Sezione di Genova[a]; Dipartimento di Fisica, Università di Genova[b], I-16146 Genova, Italy*
[25]*Indian Institute of Technology Guwahati, Guwahati, Assam, 781 039, India*
[26]*Harvard University, Cambridge, Massachusetts 02138, USA*
[27]*Harvey Mudd College, Claremont, California 91711*
[28]*Universität Heidelberg, Physikalisches Institut, Philosophenweg 12, D-69120 Heidelberg, Germany*
[29]*Humboldt-Universität zu Berlin, Institut für Physik, Newtonstr. 15, D-12489 Berlin, Germany*
[30]*Imperial College London, London, SW7 2AZ, United Kingdom*
[31]*University of Iowa, Iowa City, Iowa 52242, USA*
[32]*Iowa State University, Ames, Iowa 50011-3160, USA*
[33]*Johns Hopkins University, Baltimore, Maryland 21218, USA*
[34]*Laboratoire de l'Accélérateur Linéaire, IN2P3/CNRS et Université Paris-Sud 11, Centre Scientifique d'Orsay, B. P. 34, F-91898 Orsay Cedex, France*
[35]*Lawrence Livermore National Laboratory, Livermore, California 94550, USA*
[36]*University of Liverpool, Liverpool L69 7ZE, United Kingdom*
[37]*Queen Mary, University of London, London, E1 4NS, United Kingdom*
[38]*University of London, Royal Holloway and Bedford New College, Egham, Surrey TW20 0EX, United Kingdom*
[39]*University of Louisville, Louisville, Kentucky 40292, USA*
[40]*Johannes Gutenberg-Universität Mainz, Institut für Kernphysik, D-55099 Mainz, Germany*
[41]*University of Manchester, Manchester M13 9PL, United Kingdom*
[42]*University of Maryland, College Park, Maryland 20742, USA*
[43]*University of Massachusetts, Amherst, Massachusetts 01003, USA*
[44]*Massachusetts Institute of Technology, Laboratory for Nuclear Science, Cambridge, Massachusetts 02139, USA*
[45]*McGill University, Montréal, Québec, Canada H3A 2T8*
[46]*INFN Sezione di Milano[a]; Dipartimento di Fisica, Università di Milano[b], I-20133 Milano, Italy*
[47]*University of Mississippi, University, Mississippi 38677, USA*
[48]*Université de Montréal, Physique des Particules, Montréal, Québec, Canada H3C 3J7*
[49]*INFN Sezione di Napoli[a]; Dipartimento di Scienze Fisiche, Università di Napoli Federico II[b], I-80126 Napoli, Italy*
[50]*NIKHEF, National Institute for Nuclear Physics and High Energy Physics, NL-1009 DB Amsterdam, The Netherlands*
[51]*University of Notre Dame, Notre Dame, Indiana 46556, USA*
[52]*Ohio State University, Columbus, Ohio 43210, USA*
[53]*University of Oregon, Eugene, Oregon 97403, USA*

[54] INFN Sezione di Padova[a]; Dipartimento di Fisica, Università di Padova[b], I-35131 Padova, Italy
[55] Laboratoire de Physique Nucléaire et de Hautes Energies,
IN2P3/CNRS, Université Pierre et Marie Curie-Paris6,
Université Denis Diderot-Paris7, F-75252 Paris, France
[56] INFN Sezione di Perugia[a]; Dipartimento di Fisica, Università di Perugia[b], I-06100 Perugia, Italy
[57] INFN Sezione di Pisa[a]; Dipartimento di Fisica,
Università di Pisa[b]; Scuola Normale Superiore di Pisa[c], I-56127 Pisa, Italy
[58] Princeton University, Princeton, New Jersey 08544, USA
[59] INFN Sezione di Roma[a]; Dipartimento di Fisica,
Università di Roma La Sapienza[b], I-00185 Roma, Italy
[60] Universität Rostock, D-18051 Rostock, Germany
[61] Rutherford Appleton Laboratory, Chilton, Didcot, Oxon, OX11 0QX, United Kingdom
[62] CEA, Irfu, SPP, Centre de Saclay, F-91191 Gif-sur-Yvette, France
[63] SLAC National Accelerator Laboratory, Stanford, California 94309 USA
[64] University of South Carolina, Columbia, South Carolina 29208, USA
[65] Southern Methodist University, Dallas, Texas 75275, USA
[66] Stanford University, Stanford, California 94305-4060, USA
[67] State University of New York, Albany, New York 12222, USA
[68] Tel Aviv University, School of Physics and Astronomy, Tel Aviv, 69978, Israel
[69] University of Tennessee, Knoxville, Tennessee 37996, USA
[70] University of Texas at Austin, Austin, Texas 78712, USA
[71] University of Texas at Dallas, Richardson, Texas 75083, USA
[72] INFN Sezione di Torino[a]; Dipartimento di Fisica Sperimentale, Università di Torino[b], I-10125 Torino, Italy
[73] INFN Sezione di Trieste[a]; Dipartimento di Fisica, Università di Trieste[b], I-34127 Trieste, Italy
[74] IFIC, Universitat de Valencia-CSIC, E-46071 Valencia, Spain
[75] University of Victoria, Victoria, British Columbia, Canada V8W 3P6
[76] Department of Physics, University of Warwick, Coventry CV4 7AL, United Kingdom
[77] University of Wisconsin, Madison, Wisconsin 53706, USA

(Dated: March 15, 2011)

The decay width and mass of the $D_{s1}(2536)^+$ meson are measured via the decay channel $D_{s1}^+ \to D^{*+}K_S^0$ using $385\,\mathrm{fb}^{-1}$ of data recorded with the *BABAR* detector in the vicinity of the $\Upsilon(4S)$ resonance at the PEP-II asymmetric-energy electron-positron collider. The result for the decay width is $\Gamma(D_{s1}^+) = 0.92 \pm 0.03\,(\mathrm{stat.}) \pm 0.04\,(\mathrm{syst.})\,\mathrm{MeV}$. For the mass, a value of $m(D_{s1}^+) = 2535.08 \pm 0.01\,(\mathrm{stat.}) \pm 0.15\,(\mathrm{syst.})\,\mathrm{MeV}/c^2$ is obtained. The mass difference between the D_{s1}^+ and the D^{*+} is measured to be $m(D_{s1}^+) - m(D^{*+}) = 524.83 \pm 0.01\,(\mathrm{stat.}) \pm 0.04\,(\mathrm{syst.})\,\mathrm{MeV}/c^2$, representing a significant improvement compared to the current world average. The unnatural spin-parity assignment for the D_{s1}^+ meson is confirmed.

PACS numbers: 14.40.Lb, 13.25.Ft, 13.66.Bc

I. INTRODUCTION

The theoretical description of D_s^+ mesons is problematic because, unlike D mesons, the masses and widths of the $D_{s0}^*(2317)^+$ and $D_{s1}(2460)^+$ states [1–6] are not in agreement with potential model calculations based on HQET [7]. Theoretical explanations for the discrepancy invoke $D^{(*)}K$ molecules [8], chiral partners [9, 10], unitarized chiral models [11, 12], tetraquarks [13, 14], and lattice calculations [15, 16], but a satisfactory description is still lacking (see [17, 18] for more details). Improved measurements of the $D_{s1}(2536)^+$ meson parameters can lead to a better understanding of these states.

In this analysis a precise measurement of the $D_{s1}(2536)^+$ mass and decay width is performed based on a high statistics data sample [19]. The $D_{s1}(2536)^+$ meson, referred to as the D_{s1}^+ below, was first seen in $c\bar{c}$-continuum reactions [20], and more recently in B decays. The current world average mass value published by the Particle Data Group is based on measurements with large statistical and systematic uncertainties: $2535.29 \pm 0.20\,\mathrm{MeV}/c^2$ [21]; the mass difference between the D_{s1}^+ and the D^{*+} meson has been measured to be $525.04 \pm 0.22\,\mathrm{MeV}/c^2$ [21]. An upper limit on the decay width ($\Gamma < 2.3\,\mathrm{MeV}$ at 90% confidence level), and a measurement of the spin-parity of the D_{s1}^+ meson ($J^P = 1^+$), have been obtained, but based on low-statistics data samples only [21–23]. The mixing between the D_{s1}^+ meson and the other $J^P = 1^+$ state $D_{s1}(2460)^+$ was investigated in Ref. [24].

This analysis is based on a data sample corresponding

*Now at Temple University, Philadelphia, Pennsylvania 19122, USA
†Also with Università di Perugia, Dipartimento di Fisica, Perugia, Italy
‡Now at University of South Alabama, Mobile, Alabama 36688, USA
§Also with Università di Sassari, Sassari, Italy

to an integrated luminosity of $349\,\mathrm{fb}^{-1}$ recorded at the $\Upsilon(4S)$ resonance and $36\,\mathrm{fb}^{-1}$ recorded 40 MeV below that resonance with the *BABAR* detector at the asymmetric-energy e^+e^- collider PEP-II at the SLAC National Accelerator Laboratory. In this analysis, D_{s1}^+ mesons are reconstructed from $c\overline{c}$ continuum events in the $D^{*+}K_S^0$ channel; those originating from B decays are rejected.

The *BABAR* detector is described briefly in Sec. II. The principal criteria used in the reconstruction of the $D^{*+}K_S^0$ mass spectrum and the selection of D_{s1}^+-candidates are discussed in Sec. III. The relevant Monte Carlo (MC) simulations are described in Sec. IV, while the detector resolution parametrization is considered in Sec. V. Measurements of the mass and total width for the D_{s1}^+ state are obtained from a fit to the $D^{*+}K_S^0$ invariant mass distribution as discussed in Sec. VI. Decay angle distributions are studied in Sec. VII, where the implications for the spin-parity of the D_{s1}^+ state are also discussed. Sources of systematic uncertainty are described in Sec. VIII, and the results of the analysis are summarized in Secs. IX and X.

II. THE *BABAR* DETECTOR

The *BABAR* detector is described in detail elsewhere [25]. Charged particles are detected, and their momenta measured, with a combination of five layers of double-sided silicon microstrip detectors (SVT) and a 40-layer cylindrical drift chamber (DCH), both coaxial with the cryostat of a superconducting solenoidal magnet that produces a magnetic field of 1.5 T. Charged particle identification is achieved by measurements of the energy loss dE/dx in the tracking devices and with an internally reflecting, ring-imaging Cherenkov detector. The energy of photons and electrons is measured with a CsI(Tl) electromagnetic calorimeter, covering 90% of the 4π solid angle in the $\Upsilon(4S)$ rest frame. The instrumented flux return of the magnetic field is used to identify muons and K_L^0's.

III. SELECTION AND RECONSTRUCTION OF EVENTS

The D_{s1}^+ is reconstructed via its decay mode $D^{*+}K_S^0$, with $K_S^0 \to \pi^+\pi^-$ and $D^{*+} \to D^0\pi^+$. The D^0 is reconstructed through two decay modes, $K^-\pi^+$ and $K^-\pi^+\pi^+\pi^-$, which will be labeled $K4\pi$ and $K6\pi$, respectively, in the following. To improve the mass resolution, the mass difference $\Delta m(D_{s1}^+) = m(D_{s1}^+) - m(D^{*+}) - m(K_S^0)$ is examined.

Events are selected by requiring at least five charged tracks, at least one of which is identified as a charged kaon. Also, at least one neutral kaon candidate is required. Each track must approach the nominal e^+e^- interaction point to within 1.5 cm in the transverse direction, and to within 10 cm in the longitudinal (beam) direction. Kaon candidates are identified using the normalized kaon, pion and proton likelihood values (L_K, L_π and L_p) obtained from the particle identification system, by requiring $L_K/(L_K+L_\pi) > 0.50$ and $L_K/(L_K+L_p) > 0.018$. Furthermore, the track must be inconsistent with the electron hypothesis or have a momentum less than $0.4\,\mathrm{GeV}/c$. Tracks that fulfill $L_K/(L_K+L_\pi) < 0.98$ and $L_p/(L_p+L_\pi) < 0.98$ are selected as pions.

Candidates for the D^0 decay are formed by selecting all $K^-\pi^+$ pairs ($K^-\pi^+\pi^+\pi^-$ combinations in the second mode) that have an invariant mass within ± 100 MeV/c^2 of the nominal mass [21]. Candidates for the D^{*+} decay are formed by adding a π^+ to the D^0, such that the mass difference between D^{*+} and D^0 is less than $170\,\mathrm{MeV}/c^2$. A K_S^0 candidate consists of a π^+ π^- pair with invariant mass within $\pm 25\,\mathrm{MeV}/c^2$ of the nominal mass [21]. A kinematic fit is applied to the complete decay chain, constraining the D_{s1}^+ candidate vertex to be consistent with the e^+e^- interaction region. Mass constraints are not applied to intermediate states. Those D_{s1}^+ candidates with a χ^2 fit probability greater than 0.1% are retained. To suppress combinatorial background and events from B-decays, we require the momentum $p^*(D_{s1}^+)$ of the D_{s1}^+ in the $\Upsilon(4S)$ center-of-mass (CM) frame to exceed $2.7\,\mathrm{GeV}/c$.

The $K\pi$ and $K\pi\pi\pi$ mass spectra for accepted D^0 candidates, shown in Figs. 1(a) and 1(d), are fitted with a signal function consisting of a sum of two Gaussians with a common mean value, and a linear background function. The width of the signal regions for D^0, D^{*+} and K_S^0 candidates is defined as twice the full width at half maximum (FWHM) of the signal line shapes. A signal window of ± 18 (14) MeV/c^2 for the $K4\pi$ ($K6\pi$) mode around the mean mass of 1863.5 (1863.5) MeV/c^2 obtained from the fit is used to select D^0 candidates. For these candidates, the $D^0\pi^+ - D^0$ mass difference distributions are shown in Figs. 1(b) and 1(e). These are fitted with the sum of a relativistic Breit-Wigner signal function and a background function consisting of a polynomial times an exponential function. A D^{*+} signal region of $\pm 1\,\mathrm{MeV}/c^2$ around the fitted mean value of $145.4\,\mathrm{MeV}/c^2$ is chosen for both decay modes. To further reduce the background, the angle between the flight direction of the K_S^0 candidate and the line connecting the e^+e^- interaction point and the K_S^0 decay vertex is required to be less than 0.15 radians. For candidates passing these selection criteria, the K_S^0 candidate invariant mass distributions (Figs. 1(c) and 1(f)) are fitted with the sum of a signal function, consisting of the sum of two Gaussians, and a linear background function. A signal window of $\pm 6\,\mathrm{MeV}/c^2$ around the fitted mean mass of $497.2\,\mathrm{MeV}/c^2$ is selected for both decay modes.

In the case of an event with multiple candidates, the candidate with the best fit probability is chosen. The $\Delta m(D_{s1}^+)$ candidate spectra after all selection criteria are shown in Figs. 2(a) and 2(b). The fits to these spectra use a Double-Gaussian signal function and a linear background function. Note that for this preliminary fit the intrinsic width and the resolution are not taken into account. The FWHM values obtained are (2.2 ± 0.1) MeV

and (2.0 ± 0.1) MeV, respectively, with corresponding signal yields of about 3500 and 4000 entries.

IV. MONTE CARLO SIMULATION AND COMPARISON WITH DATA

Monte Carlo events are generated for $D_{s1}^+ \to D^{*+}K_S^0, D^{*+} \to D^0\pi^+$, with $D^0 \to K^-\pi^+$ and $D^0 \to K^-\pi^+\pi^+\pi^-$, by `EvtGen` [26]. The detector response is simulated using the `GEANT4` [27] package. For each D^0 decay mode, and for each of the corresponding D_{s1}^- decays, 776000 events are generated. The D_{s1}^+ line shape is generated using a non-relativistic Breit-Wigner function having central value $m(D_{s1}^+)_{gen} = 2535.35\,\mathrm{MeV}/c^2$ and intrinsic width $\Gamma(D_{s1}^+)_{gen} = 1\,\mathrm{MeV}$ (this sample is labeled Γ_1 in the following). The range of generated D_{s1}^+ masses is restricted to values between $m(D_{s1}^+)_{gen} - 10\,\mathrm{MeV}/c^2$ and $m(D_{s1}^+)_{gen} + 15\,\mathrm{MeV}/c^2$. The masses of the daughter particles are taken from Ref. [21].

In order to test the mass resolution model, a second set of MC samples with 381000 events for each D^0 decay mode is generated using a Breit-Wigner width of $\Gamma(D_{s1}^+)_{gen} = 2\,\mathrm{MeV}$ (Γ_2 sample). In addition to these signal MC samples, separate D^0 and K_S^0 samples are created from data and generic $c\overline{c}$ MC simulations without requiring a D^{*+} or D_{s1}^+. They are used mainly for resolution studies.

The MC and data are in good agreement for the transverse momentum distributions of pions, kaons, D and D^* mesons, and for the number of SVT coordinates of pions and kaons. The agreement is worse for the number of DCH coordinates, where the data show systematically fewer coordinates than the MC, giving rise to a resolution that is about 10% smaller in the MC than in data. This is illustrated in Fig. 3, which shows the $p^*(K_S^0)$ and $p^*(D^0)$ dependence of the ratio between the FWHM of the resolution functions in $c\overline{c}$ MC and data, where p^* is the momentum in the CM frame. This effect will be discussed further in Sec. VIII. There is also disagreement between the number of D_{s1}^+ signal entries in MC and data as a function of $p^*(D_{s1}^+)$ (Fig. 4). This effect will be addressed in Secs. V and VIII.

V. RESOLUTION MODEL

The resolution model is derived from the D_{s1}^+ signal MC by studying the difference Δm_{res} between the reconstructed and generated D_{s1}^+ mass values. The Multi-Gaussian ansatz

$$G(\Delta m_{res}) = \int_{\sigma_0}^{r\sigma_0} \frac{1}{r\sigma^2} e^{-\frac{(\Delta m_{res} - \Delta m_{res0})^2}{2\sigma^2}} \mathrm{d}\sigma \qquad (1)$$

is found to accurately model the mass resolution spectra. This represents a superposition of Gaussian distributions with the same mean value Δm_{res0} but variable width σ, starting from minimum width σ_0 and increasing to maximum width $r\sigma_0$. The FWHM of the distribution is numerically calculable once σ_0 and r are known. The mass resolution for the different particles depends on the CM momentum $p^*(D_{s1}^+)$. Therefore, the parameter σ_0 of Eq. (1) is obtained as a function of $p^*(D_{s1}^+)$.

Figures 5(a) and 5(b) show Δm_{res} distributions for the full $p^*(D_{s1}^+)$ range. From these plots the value of the parameter r is determined to be 4.78 ± 0.04 and 5.20 ± 0.05 for the $K4\pi$ and $K6\pi$ modes, respectively. Events are divided into 30 $p^*(D_{s1}^+)$ intervals from $2.7\,\mathrm{GeV}/c$ to $4.7\,\mathrm{GeV}/c$ and the fit repeated for each interval, resulting in $p^*(D_{s1}^+)$-dependent σ_0 values (Figs. 6(a) and 6(b)). The corresponding $p^*(D_{s1}^+)$-dependent FWHM of the resolution functions is shown in Figs. 7(a) and 7(b).

In order to validate this resolution model, the $p^*(D_{s1}^+)$-dependent resolution function with the corresponding parameters σ_0 and r is convolved with a non-relativistic Breit-Wigner function and fitted to the $\Delta m(D_{s1}^+)$ signal MC distribution (MC sample Γ_1). The results are shown in Figs. 8(a) and 8(b), and the reconstructed values for mean $\Delta m(D_{s1}^+)_0$ and width $\Gamma(D_{s1}^+)$ are listed in Table I. The corresponding generated values for both decay modes are $\Delta m(D_{s1}^+)_{gen} = 27.744\,\mathrm{MeV}/c^2$ for the mean and $\Gamma(D_{s1}^+)_{gen} = 1.000\,\mathrm{MeV}$ for the width. The small deviations between generated and reconstructed values are discussed in Sec. VIII.

TABLE I: Reconstructed values for $\Delta m(D_{s1}^+)_0$ and $\Gamma(D_{s1}^+)$ (fit to MC sample Γ_1). The resolution model used is derived from MC sample Γ_1.

	$\Delta m(D_{s1}^+)_0/\,\mathrm{MeV}/c^2$	$\Gamma(D_{s1}^+)/\,\mathrm{MeV}$
$(K4\pi)$	27.737 ± 0.003	1.001 ± 0.005
$(K6\pi)$	27.734 ± 0.003	0.991 ± 0.006

VI. FIT TO THE $D^*K_S^0$ MASS SPECTRUM

For the final fit to the $D^*K_S^0$ mass spectra, as represented by the $\Delta m(D_{s1}^+)$ distributions of Figs. 2 and 9, the signal function consists of a relativistic Breit-Wigner line shape numerically convolved with the $p^*(D_{s1}^+)$-dependent resolution function (Eq. (1)). A linear function is used to describe the background.

The relativistic Breit-Wigner function used takes the form

$$\left(\frac{p_{1,m}}{p_{1,m_0}}\right)^{2L+1} \left(\frac{m_0}{m}\right) \frac{m F_L(p_{1,m})^2}{(m_0^2 - m^2)^2 + \Gamma_m^2 m_0^2}, \qquad (2)$$

where m_0 is an abbreviation for $\Delta m(D_{s1}^+)_0$ and m stands for $\Delta m(D_{s1}^+)$. The variable $p_{1,m}$ is the momentum of the D^{*+} in the rest frame of the D_{s1}^+ resonance candidate, which has mass m, and p_{1,m_0} is the value for $m = m_0$. The respective Blatt-Weisskopf barrier factors $F_L(p_{1,m})$ for orbital angular momentum L between the D^{*+} and

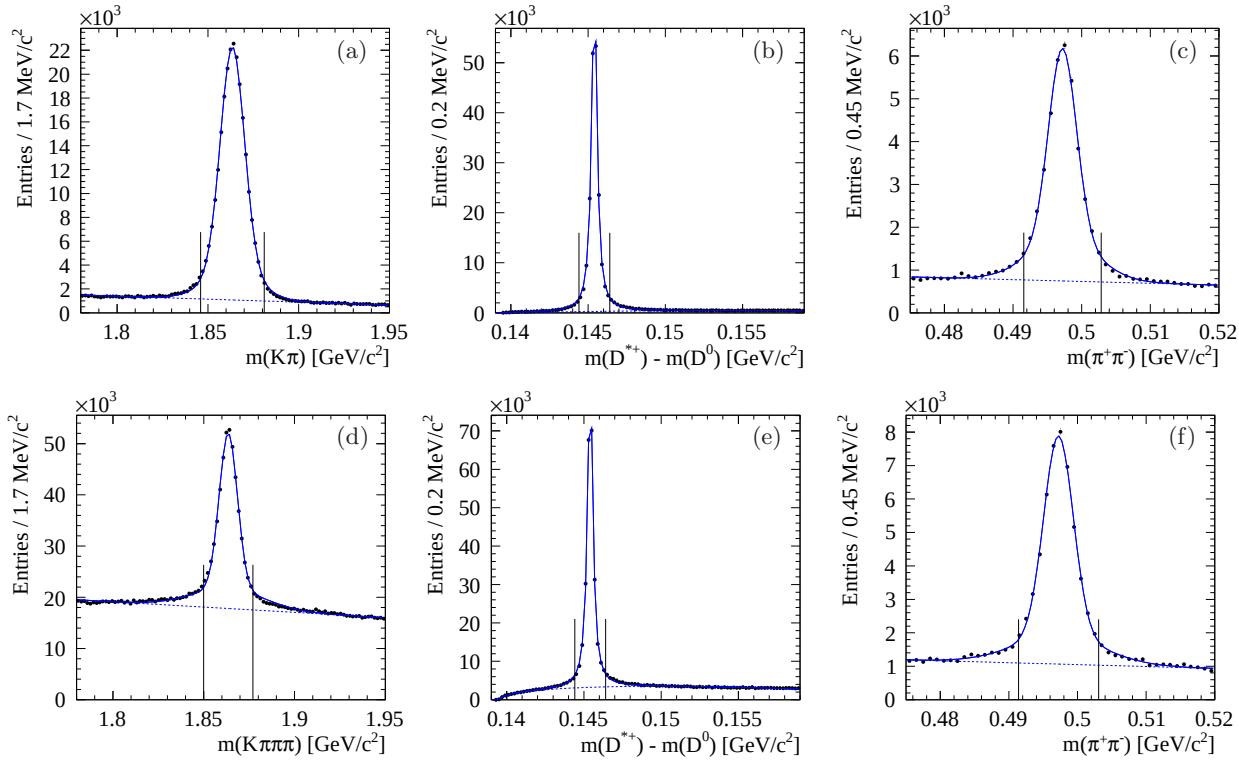

FIG. 1: (a,d) D^0 candidate invariant mass distributions; (b,e) Difference between the D^{*+} and D^0 candidate invariant masses. (c,f) K^0_S candidate invariant mass distributions; (a-c) $K4\pi$ mode; (d-f) $K6\pi$ mode. Signal regions are indicated by the vertical lines. The signal and background line shapes fitted to the mass distributions are described in the text.

K^0_S are

$$F_0(p_{1,m}) = 1, \quad (3)$$

$$F_1(p_{1,m}) = \frac{\sqrt{1+(Rp_{1,m_0})^2}}{\sqrt{1+(Rp_{1,m})^2}}, \quad (4)$$

$$F_2(p_{1,m}) = \frac{\sqrt{9+3(Rp_{1,m_0})^2+(Rp_{1,m_0})^4}}{\sqrt{9+3(Rp_{1,m})^2+(Rp_{1,m})^4}}, \quad (5)$$

where

$$R = 1.5\ (\mathrm{GeV}/c)^{-1} \quad (6)$$

is defined as in Ref. [28]. The mass-dependent width is given by

$$\Gamma_m = \Gamma(D^+_{s1})\left(\mathcal{B}_1\left(\frac{p_{1,m}}{p_{1,m_0}}\right)^{2L+1}\left(\frac{m_0}{m}\right)F_L(p_{1,m})^2 + \mathcal{B}_2\left(\frac{p_{2,m}}{p_{2,m_0}}\right)^{2L+1}\left(\frac{m_0}{m}\right)F_L(p_{2,m})^2\right) \quad (7)$$

with $\Gamma(D^+_{s1})$ the total intrinsic width of the D^+_{s1} resonance. This relation takes into account the $D^+_{s1} \to D^{*+}K^0$ and the $D^+_{s1} \to D^{*0}K^+$ decay modes, with the corresponding branching fractions $\mathcal{B}_1$ and $\mathcal{B}_2$, respectively:

$$\mathcal{B}_i = \frac{p^{2L+1}_{i,m_0}}{p^{2L+1}_{1,m_0}+p^{2L+1}_{2,m_0}}. \quad (8)$$

Since the D^+_{s1} mass lies close to threshold for both decay modes, the mass values of the decay particles make a significant difference. The momenta $p_{2,m}$ and p_{2,m_0} correspond to $p_{1,m}$ and p_{1,m_0}, respectively, but are calculated for the $D^{*0}K^+$ decay mode.

It is assumed that the D^+_{s1} has spin-parity $J^P = 1^+$ and from parity conservation that the orbital angular momentum L is either 0 or 2. The S-wave usually dominates in 1^+ decays, so $L = 0$ is chosen for the main fit and an additional $L = 2$ contribution is used to estimate a systematic uncertainty. Further discussion on the J and L values is presented in Sec. VII.

The fit to the $\Delta m(D^+_{s1}) = m(D^+_{s1}) - m(D^*) - m(K^0_S)$ mass difference spectrum in data (Fig. 9) yields mean mass differences

$$\Delta m(D^+_{s1})_0 = 27.231 \pm 0.020\,\mathrm{MeV}/c^2 \quad (K4\pi),$$
$$\Delta m(D^+_{s1})_0 = 27.205 \pm 0.018\,\mathrm{MeV}/c^2 \quad (K6\pi),$$

and total width values

$$\Gamma(D^+_{s1}) = 1.000 \pm 0.049\,\mathrm{MeV} \quad (K4\pi),$$
$$\Gamma(D^+_{s1}) = 0.941 \pm 0.045\,\mathrm{MeV} \quad (K6\pi).$$

The fitted values for the two D^0 decay modes agree within the statistical errors. The signal yield is 3704 ± 71 for $K4\pi$ and 4334 ± 78 for $K6\pi$.

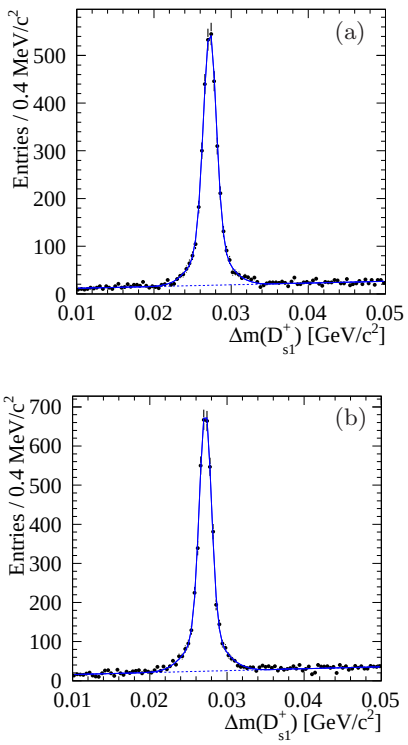

FIG. 2: $\Delta m(D_{s1}^+) = m(D_{s1}^+) - m(D^{*+}) - m(K_S^0)$ invariant mass distributions in data after applying all selection criteria for the (a) $K4\pi$ and (b) $K6\pi$ mode. A Double-Gaussian signal function and a linear background function are used to describe the data in a preliminary fit.

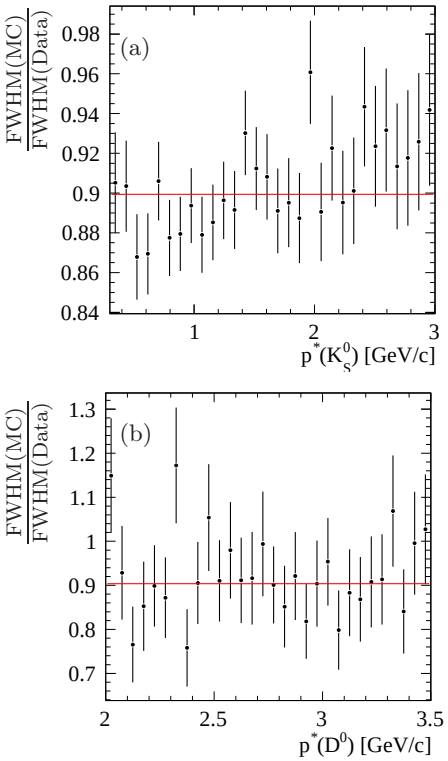

FIG. 3: p^*-dependence of the ratio between the FWHM of the resolution functions from $c\bar{c}$-MC and data. (a) $K_S^0 \to \pi^+\pi^-$. (b) $D^0 \to K^-\pi^+\pi^+\pi^-$. The solid line shows the fitted mean ratio with a value of 0.9.

VII. ANGULAR DISTRIBUTION

The assigned spin-parity $J^P = 1^+$ of the D_{s1}^+ is based on studies with small data samples (less than 200 reconstructed events) [22, 23]. There, fits of an angular distribution corresponding to unnatural spin-parity $(1^+, 2^-, \ldots)$ yielded the highest confidence level. In this analysis clean signals with a total number of about 8000 reconstructed D_{s1}^+-candidates are available, making a detailed study possible.

***D*$^{*+}$ decay angle.** Since in this analysis the origin of the D_{s1}^+ is not known, the decay angle θ' between the D^0 momentum vector in the D^{*+} CM system and the D^{*+} momentum vector in the D_{s1}^+ CM system (Fig. 10a) is used for the J^P analysis. The resulting angular distribution $dN(D_{s1}^+)/d\cos\theta'$ is influenced by the spin of the D_{s1}^+. The expected distributions for different D_{s1}^+ spin-parity values are calculated using the helicity formalism [29–31] and are listed in Table II.

The data are corrected for the detection efficiency and divided into 20 bins of $\cos\theta'$. The signal entries for the $\cos\theta'$ bins are obtained from separate fits to the data with the mass and decay width of the D_{s1}^+ fixed to the values reported in Sec. VI. The $dN(D_{s1}^+)/d\cos\theta'$ distribution shown in Fig. 11 is the combined result from the $K4\pi$ and $K6\pi$ samples.

Comparison with the theoretical distributions shows a clear preference for the unnatural spin-parity values $J^P = 1^+, 2^-, 3^+ \ldots$, confirming the earlier results [22, 23]. The signal function for these J^P values is

$$I(\theta') = a(\sin^2\theta' + \beta\cos^2\theta'), \qquad (9)$$

where $\beta = |A_{00}|^2/|A_{10}|^2$ and a is a constant. The helicity amplitudes $|A_{00}|$ and $|A_{10}|$ correspond to the D^{*+} helicities 0 and ± 1, respectively.

The lowest value $J^P = 1^+$ is the most probable one: assuming 1^+ implies $l = 1$ (orbital momentum between the light and heavy quark), while the higher J values demand $l \geq 2$; such mesons are expected to be highly suppressed in e^+e^- production [32]. The coefficient β is 1 in the case of a pure S-wave decay of D_{s1}^+ into $D^{*+}K_S^0$, thus yielding a flat distribution in disagreement with data. The results reported in Table II for β clearly indicate a D-wave contribution. Based on the results for β, the ratio of the helicity amplitudes is determined to be $|A_{10}|/|A_{00}| = 2.09 \pm 0.09$ for the combined $K4\pi$ and $K6\pi$ samples, and 2.09 ± 0.14 and 2.04 ± 0.13 for the individual samples, respectively. The squared ratio of the amplitudes is $|A_{10}|^2/|A_{00}|^2 = 4.35 \pm 0.38$

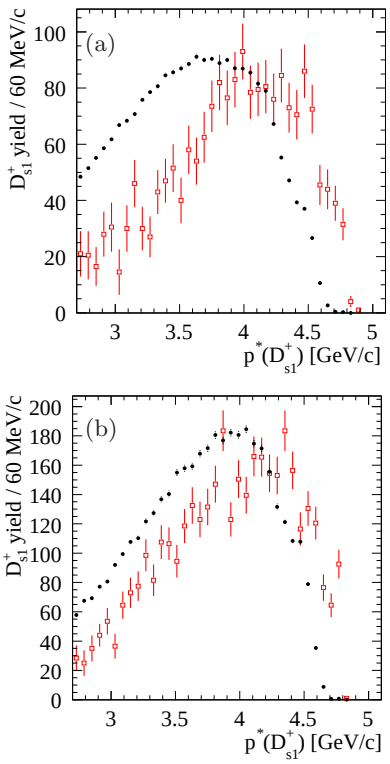

FIG. 4: $p^*(D_{s1}^+)$-dependence of the D_{s1}^+ signal yield for data (open squares) and reconstructed MC (solid points) for the (a) $K4\pi$ and (b) $K6\pi$ decay modes.

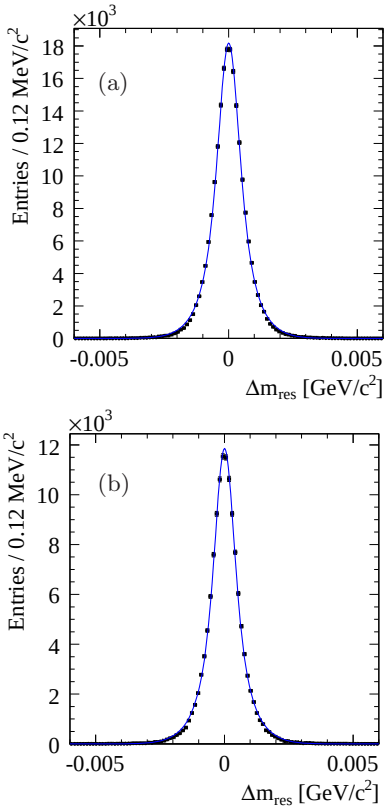

FIG. 5: Fit of the resolution function (Eq. (1)) to Δm_{res} with the r and σ_0 parameters free to vary for the (a) $K4\pi$ and (b) $K6\pi$ decay modes.

(combined data), consistent with the Belle result $|A_{10}|^2/|A_{00}|^2 = 3.6 \pm 0.3 \pm 0.1$ [24].

D_{s1}^+ decay angle. The $dN(D_{s1}^+)/d\cos\theta$ distribution is also studied, where θ is the decay angle between the D^{*+} momentum vector in the D_{s1}^+ CM system and the D_{s1}^+ momentum vector in the e^+e^- CM system (Fig. 10b). The combined efficiency-corrected $\cos\theta$ spectrum is shown in Fig. 12. The results in this figure indicate that the D_{s1}^+ decay to $D^{*+}K_S^0$ is not purely S-wave. Were this decay purely S-wave, the distribution would be flat. The $\cos\theta$ distribution, assuming $J^P = 1^+$, is

$$I(\theta) = a((1+\rho_{00})|A_{10}|^2 + (1-\rho_{00})|A_{00}|^2 + (1-3\rho_{00})(|A_{10}|^2 - |A_{00}|^2)\cos^2\theta) \quad (10)$$

where ρ_{00} gives the probability that the D_{s1}^+ helicity is zero.

Results from a fit of both a constant and a distribution proportional to $1 + t\cos^2\theta$ (based on Eq. (10)) are given in Table III. Using the value of t from the $\cos\theta$ fit, the result for $|A_{10}|^2/|A_{00}|^2$ from the $\cos\theta'$ fit, and the coefficients from Eq. (10), we determine $\rho_{00} = 0.48 \pm 0.03$ for the combined $K4\pi$ and $K6\pi$ samples, and 0.44 ± 0.04 and 0.53 ± 0.04 for the individual samples, consistent with the Belle result $\rho_{00} = 0.490 \pm 0.012$ [24].

Several effects that might affect the results of the angular analysis have been studied.

Test for non-flat efficiency. The formalism used for the calculation of $I(\theta')$ assumes a flat acceptance in $\cos\theta$. In this study, the efficiency decreases a few percent for values of $\cos\theta > 0$. In order to assess the impact of this effect, all D_{s1}^+ candidates with $\cos\theta > 0$ are removed from the data sample. The results for β from fits to the reduced $\cos\theta'$ spectra are consistent with the nominal results, ruling out an observable effect due to non-flat efficiency.

Test for possible interference. Possible interference with unreconstructed recoil particle(s) X in the decay chain $e^+e^- \to D_{s1}^+X$ is considered. The effect of interference is expected to depend on the flight direction of the D_{s1}^+. Therefore the data are divided into four subsamples based on their $\cos\theta_d$ value, where θ_d is the flight angle of the D_{s1}^+ relative to the beam axis (calculated in the e^+e^- CM system). For each of these reduced data samples, the fit to the $\cos\theta'$ distribution is repeated. The values obtained for the parameter β are fully consistent within errors with each other and with the nominal value (full data sample), ruling out a significant interference effect. The same consistency between results is found in

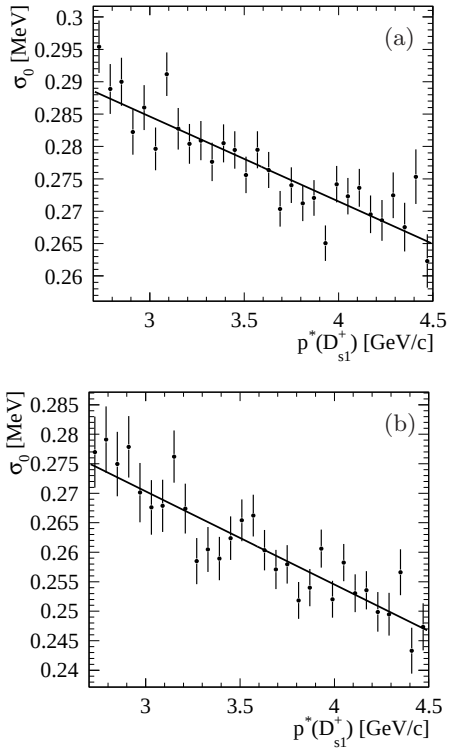

FIG. 6: $p^*(D_{s1}^+)$ dependence of the resolution function parameter σ_0, represented by a linear parametrization (r fixed) for the (a) $K4\pi$ and (b) $K6\pi$ decay modes.

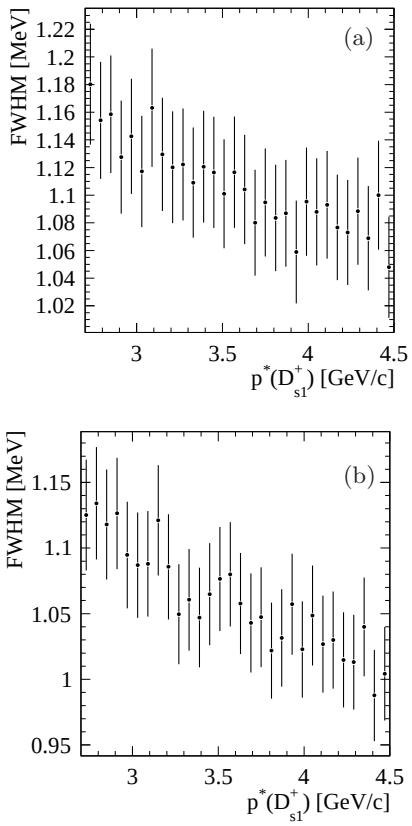

FIG. 7: $p^*(D_{s1}^+)$ dependence of the FWHM of the resolution function (r fixed) for the (a) $K4\pi$ and (b) $K6\pi$ decay modes.

fits to $\cos\theta$.

VIII. SYSTEMATIC STUDIES

The investigated sources of systematic uncertainty can be separated into three main categories: uncertainties arising from the resolution model, fit procedure, and reconstruction. The uncertainties are defined by taking the differences $\Delta_{\Delta m}$ and Δ_Γ between the standard result for the mass difference $\Delta m(D_{s1}^+)_0$ and width $\Gamma(D_{s1}^+)$ given in Sec. VI and the result obtained with the correspondent modification. A summary of the results is listed in Table IV. If not otherwise stated, the momentum-dependent resolution model and the relativistic Breit-Wigner signal function combined with a first order polynomial for background parametrization from the standard fit are used. Deviations smaller than $0.5\,\mathrm{keV}/c^2$ for $\Delta_{\Delta m}$ and smaller than 0.5 keV for Δ_Γ are considered as negligible.

A. Resolution model uncertainties

General comparison between MC and Data. The D^0 and K_S^0 test samples (see Sec. IV) demonstrate that the mass resolution is underestimated by 10% in MC (Fig. 3), yielding an overestimated decay width from the fits to data. The effect of this is quantitatively studied by increasing the width of the resolution function by 10%. The repeated fits yield no significant deviations for the mass difference, but a 51 (45) keV smaller decay width. The nominal decay width values obtained from the fits in Sec. VI are thus corrected by these values, yielding values of $\Gamma(D_{s1}^+) = 0.949$ (0.896) MeV for the $K4\pi$ ($K6\pi$) mode.

To estimate the corresponding systematic uncertainty, the resolution function modification is varied within $(10\pm 4)\%$ to take a possible p^* dependence into account (this value is derived from Fig. 3(a), which shows the largest variation in p^*). There are no effects on $\Delta m(D_{s1}^+)_0$, and a deviation of $^{-30}_{+8}$ keV for $\Gamma(D_{s1}^+)$ is observed in both decay modes, compared to the corrected results from above. As a conservative estimate, the larger deviation is used as a two-sided uncertainty, providing the largest systematic error for the decay width.

Further validation of the resolution model. To further validate the procedure used to obtain the resolution model, the results from fits to the Γ_1 and Γ_2 MC samples are compared. The derived resolution function parameters are in good agreement between the two

TABLE II: List of spin-parity values J^P for the D_{s1}^+ and the corresponding decay angle distributions for the D^{*+}. Under the assumption of a strong decay, 0^+ is forbidden. The last three columns show the χ^2/NDF of the fits to the $\cos\theta'$-distribution for efficiency-corrected data, with NDF being the number of degrees of freedom.

J^P	$dN(D_{s1}^+)/d\cos\theta'$	$\chi^2/NDF(K4\pi)$	$\chi^2/NDF(K6\pi)$	χ^2/NDF (combined data)
0^+	forbidden	–	–	–
0^-	$a\cos^2\theta'$	2142.7/19	2440.8/19	4578.0/19
$1^-, 2^+, 3^-, \ldots$	$a\sin^2\theta'$	103.2/19	108.8/19	190.9/19
$1^+, 2^-, 3^+, \ldots$ (S-wave only)	const	392.1/19	425.1/19	802.5/19
$1^+, 2^-, 3^+, \ldots$ (S-, D-wave)	$a(\sin^2\theta' + \beta\cos^2\theta')$	24.9/18	9.5/18	14.7/18
		$(\beta = 0.23 \pm 0.03)$	$(\beta = 0.24 \pm 0.03)$	$(\beta = 0.23 \pm 0.02)$

TABLE III: χ^2/NDF values of the fits to the $\cos\theta$-distribution for efficiency-corrected data, with NDF being the number of degrees of freedom.

	$dN(D_{s1}^+)/d\cos\theta$	$\chi^2/NDF(K4\pi)$	$\chi^2/NDF(K6\pi)$	χ^2/NDF (combined data)
pure S-wave	constant	19.0/19	55.5/19	57.0/19
S- and D-wave	$a(1 + t\cos^2\theta)$	12.0/18	27.3/18	25.2/18
		$(t = -0.15 \pm 0.05)$	$(t = -0.27 \pm 0.05)$	$(t = -0.21 \pm 0.04)$

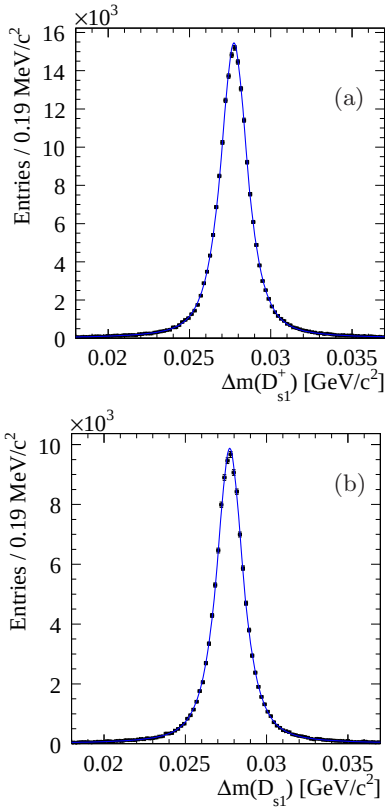

FIG. 8: Fit of a non-relativistic Breit-Wigner convolved with the resolution function to the D_{s1}^+ candidate mass difference spectra in the Γ_1 MC sample for the (a) $K4\pi$ and (b) $K6\pi$ decay modes.

samples. The widths of the reconstructed $\Delta m(D_{s1}^+)$ distributions determined from fitting the Γ_2 samples, $\Gamma(D_{s1}^+) = 2.004 \pm 0.016\,\text{MeV}$ for the $K4\pi$ mode and $2.018 \pm 0.022\,\text{MeV}$ for the $K6\pi$ mode, are in good agreement with the generated values. Similarly, when the resolution function from the Γ_2 sample is used to determine the width for the Γ_1 sample, values of $\Gamma(D_{s1}^+) = 1.003 \pm 0.005\,\text{MeV}$ and $0.999 \pm 0.006\,\text{MeV}$, respectively, are obtained, in agreement with the generated values.

As a conservative estimate, the small deviations found during the validation procedure for the resolution model using the Γ_1 sample in Sec. V are used as systematic uncertainties: $\Delta_{\Delta m} = -7\ (-10)\,\text{keV}/c^2$; $\Delta_\Gamma = +1\ (-9)\,\text{keV}$ for $K4\pi$ ($K6\pi$).

Alternative resolution models. Using the resolution model obtained from the Γ_2 MC sample, a fit to data yields uncertainties $\Delta_{\Delta m} < 0.5\ (< 0.5)\,\text{keV}/c^2$ and $\Delta_\Gamma = +1\ (+12)\,\text{keV}$ for $K4\pi$ ($K6\pi$).

Instead of the momentum-dependent resolution model of the standard analysis, an alternative model has been tested, based on the comparison of MC and data distributions that show disagreement, such as the $p^*(D_{s1}^+)$ dependence of the D_{s1}^+ yield. By dividing the MC and data spectra from Fig. 4, a correction function is derived. MC data are modified with this function such that the two distributions in Fig. 4 coincide. From these corrected MC, a new resolution model is derived. The results for $\Delta m(D_{s1}^+)_0$ and $\Gamma(D_{s1}^+)$ in data agree within the error with the momentum-dependent treatment (systematic uncertainties $\Delta_{\Delta m} < 0.5\ (< 0.5)\,\text{keV}/c^2, \Delta_\Gamma = -2\ (+1)\,\text{keV}$ for $K4\pi$ ($K6\pi$)).

The larger deviations listed above are reported as the systematic uncertainties associated with the use of alternative resolution models.

Parameters of the $p^*(D_{s1}^+)$-dependent resolution model. The parameter r of the $p^*(D_{s1}^+)$-dependent resolution model is modified within its er-

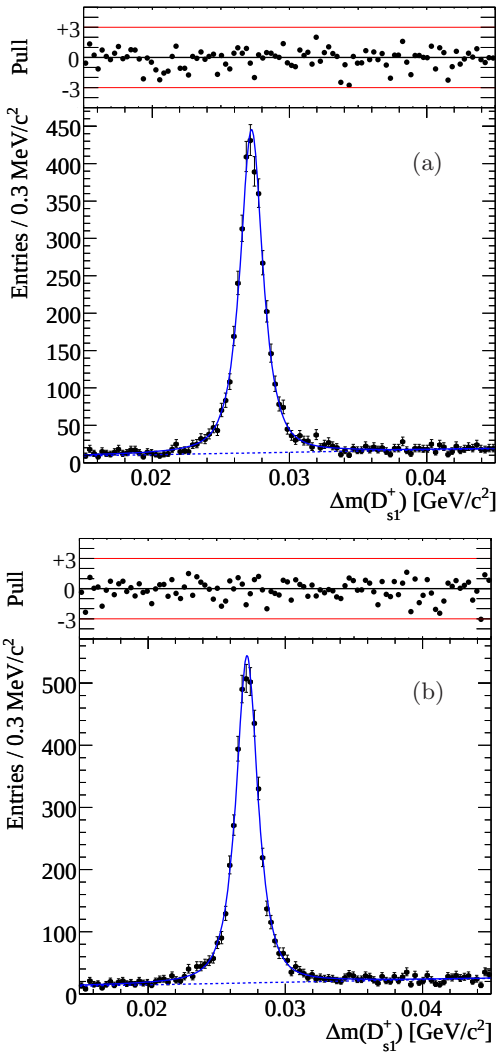

FIG. 9: Fit of a relativistic Breit-Wigner convolved with the resolution function to the D_{s1}^+ candidate mass difference spectra in data, for the (a) $K4\pi$ and (b) $K6\pi$ modes. The dotted line indicates the background line shape. The upper parts of the figures show the normalized fit residuals.

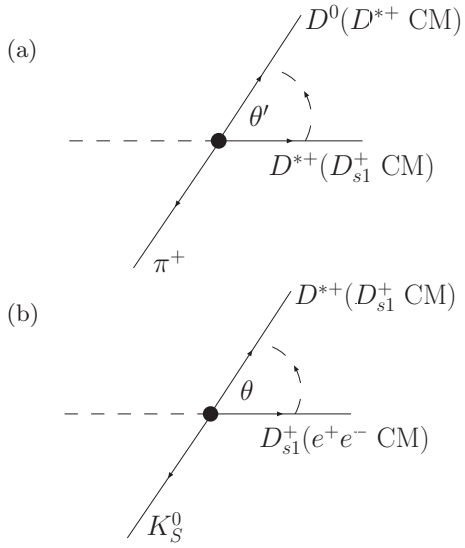

FIG. 10: a) Decay angle θ' of the D^{*+}. b) Decay angle θ of the D_{s1}^+.

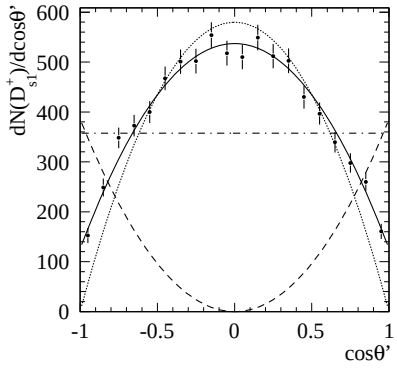

FIG. 11: Efficiency-corrected signal yield as function of $\cos\theta'$ in data. The following models are fitted to the distribution: $a(\sin^2\theta' + \beta\cos^2\theta')$ (solid line); a constant (dash-dotted line); $a\cos^2\theta'$ (dashed line); $a\sin^2\theta'$ (dotted line).

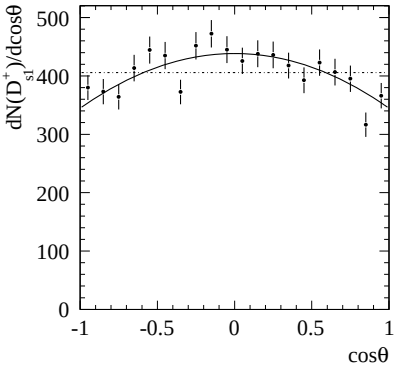

FIG. 12: Efficiency-corrected signal yield as function of $\cos\theta$ in data. The following models are fitted to the distribution: constant (dotted line); $a(1 + t\cos^2\theta)$ (solid line).

ror leading to negligible deviations in $\Delta m(D_{s1}^+)_0$ and ± 6 (± 7) keV in $\Gamma(D_{s1}^+)$ for $K4\pi$ ($K6\pi$). A different parametrization of the $\sigma_0(p^*(D_{s1}^+))$-dependence (second order polynomial) results in a negligible deviation for $\Delta m(D_{s1}^+)_0$ and -3 (-2) keV for $\Gamma(D_{s1}^+)$.

B. Fit Procedure Uncertainties

Breit-Wigner line shape. In the standard fit, a pure S-wave decay of the D_{s1}^+ to $D^{*+}K_S^0$ is assumed, using a Breit-Wigner line shape corresponding to $L = 0$. To estimate a systematic uncertainty, a combination of an S-wave and a D-wave Breit-Wigner is used instead. Relative contributions of 72% and 28% are used, based on a decay angle analysis of the D_{s1}^+ by the Belle Collabora-

tion [24]. Using the modified signal lineshape, uncertainties of -9 $(-8)\,\mathrm{keV}/c^2$ in $\Delta m(D_{s1}^+)_0$ and -2 $(-3)\,\mathrm{keV}$ in $\Gamma(D_{s1}^+)$ are derived, compared with the standard results.

As an additional check, the value of R (Eq. (6)) is set to 2.0 $(\mathrm{GeV}/c)^{-1}$. No effect on $\Delta m(D_{s1}^+)_0$ and $\Gamma(D_{s1}^+)$ is observed.

The effect of neglecting $D^{*0}K^+$ decays (Sec. VI) is studied by setting $\mathcal{B}_1 = 1$ and $\mathcal{B}_2 = 0$. The resulting uncertainties are negligible for both $\Delta m(D_{s1}^+)_0$ and $\Gamma(D_{s1}^+)$.

Numerical precision of convolution. The integration range and number of steps in the numerical convolution of the signal line shape and resolution function (Sec. VI) are varied, resulting in a negligible deviation both for the mass and the width.

Mass window. The mass window for $\Delta m(D_{s1}^+)$ is enlarged, resulting in no significant change for $\Delta m(D_{s1}^+)_0$ and a difference for the width of $\Delta_\Gamma = +9$ $(+3)\,\mathrm{keV}$.

Background parametrization. For background parametrization, a power law function proportional to m^α is used instead of a linear function, leaving $\Delta m(D_{s1}^+)_0$ unaffected but yielding $\Delta_\Gamma = -5$ $(-7)\,\mathrm{keV}$ for $K4\pi$ $(K6\pi)$.

C. Reconstruction Uncertainties

Tracking region material. Uncertainties in the D_{s1}^+ mass may arise from uncertainties in the energy-loss correction in charged particle tracking. Studies of Λ and K_S^0 decays suggest that the correction might be underestimated [33]. Two possibilities are considered, one with the SVT material density increased by 20% and the other with the tracking region material density (SVT, DCH) increased by 10%, as was investigated in detail in Refs. [4, 33]. The deviations indicate that the fit results for the mass might be underestimated. The larger values from the two studies ($\Delta_{\Delta m} = +21$ $(+13)\,\mathrm{keV}/c^2$ and $\Delta_\Gamma = +14$ $(-15)\,\mathrm{keV}$ for $K4\pi$ $(K6\pi)$) are chosen as a two-sided systematic uncertainty.

SVT alignment. Slight possible deviations in the alignment of SVT components may affect the measurement of angles between tracks and thus the mass measurement. This is studied by applying small distortions to the SVT alignment in simulated data, comprising general changes between different run periods and radial shifts. Results are $\Delta_{\Delta m} = \pm 6$ $(\pm 7)\,\mathrm{keV}/c^2$ and $\Delta_\Gamma = \pm 2$ $(\pm 14)\,\mathrm{keV}$ for $K4\pi$ $(K6\pi)$.

Magnetic field. The magnetic field inside the tracking volume has several components: the main solenoidal field, fields from permanent magnets and an additional magnetization of the latter due to the main field. To understand the effect of the field on the track reconstruction, the solenoid field strength is varied by $\pm 0.02\%$ and the magnetization of the permanent magnets by $\pm 20\%$ [4, 33]. For the mass difference, the larger deviations arising from the change in rescaled solenoid field and magnetization are added in quadrature and the sum is assigned as a systematic uncertainty associated with the magnetic field; the same is done for the decay width. The results are $\Delta_{\Delta m} = \pm 13$ $(\pm 19)\,\mathrm{keV}/c^2$ and $\Delta_\Gamma = \pm 19$ $(\pm 11)\,\mathrm{keV}$ for $K4\pi$ $(K6\pi)$.

Distance scale. A further source of uncertainty for the momentum determination comes from the distance scale. The positions of the signal wires in the drift chamber are known with a precision of $40\,\mu\mathrm{m}$, corresponding to a relative precision of 0.01%. As an estimate of the uncertainty of the momentum due to the distance scale, a systematic error half the size of the uncertainty obtained from the 0.02% variation of the solenoid field is assigned. For the mass difference this yields a shift of ± 4 $(\pm 6)\,\mathrm{keV}/c^2$ for $K4\pi$ $(K6\pi)$; the width is shifted by ± 8 $(\pm 4)\,\mathrm{keV}$ for $K4\pi$ $(K6\pi)$.

Drift Chamber hits. In the standard D_{s1}^+ selection no lower limit is set for the number of drift chamber hits. Requiring at least 20 hits per track, thereby excluding the low momentum pions from D^{*+} decays, modifies $\Delta m(D_{s1}^+)_0$ by -11 $(-15)\,\mathrm{keV}/c^2$ and $\Gamma(D_{s1}^+)$ by -7 $(-7)\,\mathrm{keV}$ for $K4\pi$ $(K6\pi)$.

Angular dependence. For the reconstructed K_S^0 and D^0 masses from the test data samples (see Sec. IV), a sine-like dependence on the azimuthal angle ϕ is observed. This effect was also observed in a previous *BABAR* analysis and might be related to the internal alignment of the DCH [33]. For a detailed study, the same ϕ-dependence is introduced into the signal MC samples by modifying the kaon and pion track momenta accordingly. Due to symmetry, the effect disappears when all ϕ angles are taken into account, but as a conservative estimate the amplitude of the sine-like shift on the reconstructed D_{s1}^+ mass in MC (13 (14) keV/c^2 for $K4\pi$ $(K6\pi)$) is taken as a systematic error for $\Delta m(D_{s1}^+)_0$.

IX. RESULTS

For the combination of the measurements, a Best Linear Unbiased Estimate (BLUE, [34]) technique is used, where correlations between the systematic uncertainties are taken into account. Adding the nominal D^{*+} and K_S^0 masses, $2010.25\,\mathrm{MeV}/c^2$ and $497.614\,\mathrm{MeV}/c^2$ (with their respective errors of $0.140\,\mathrm{MeV}/c^2$ and $0.024\,\mathrm{MeV}/c^2$ [21]), the final value for the D_{s1}^+ mass is

$$m(D_{s1}^+) = 2535.08 \pm 0.15\,\mathrm{MeV}/c^2.$$

Using a slightly different method for the combination of the individual results [4], a value of

$$m(D_{s1}^+) = 2535.08 \pm 0.01 \pm 0.15\,\mathrm{MeV}/c^2$$

is obtained, where the first error denotes the statistical and the second the systematic uncertainty. The latter is dominated by the uncertainty of the D^{*+} mass. The mass difference between the D_{s1}^+ and the D^{*+} is

$$m(D_{s1}^+) - m(D^{*+}) = 524.83 \pm 0.04\,\mathrm{MeV}/c^2,$$

using the BLUE technique, and for the alternative combination method

$$m(D_{s1}^+) - m(D^{*+}) = 524.83 \pm 0.01 \pm 0.04\,\mathrm{MeV}/c^2,$$

which has a significantly smaller systematic uncertainty than the $m(D_{s1}^+)$ result.

For the total decay width of the D_{s1}^+, combining the results from the two measurements in the same way as for the mass yields

$$\Gamma(D_{s1}^+) = 0.92 \pm 0.05\,\mathrm{MeV},$$

using the BLUE technique, and for the alternative combination method

$$\Gamma(D_{s1}^+) = 0.92 \pm 0.03 \pm 0.04\,\mathrm{MeV}.$$

The corrections of -51 $(-45)\,\mathrm{keV}$ for the $K4\pi$ $(K6\pi)$ decay mode, based on the systematic resolution studies (Sec. VIII A), are applied prior to the combination process.

X. SUMMARY

In this paper, precision measurements of the mass and decay width of the charmed-strange meson $D_{s1}(2536)^+$ via the decay $D_{s1}^+ \to D^{*+}K_S^0$ are presented. Two decay modes are analyzed, with the D^0 that originates from the D^{*+} decaying either through $K^-\pi^+$ or $K^-\pi^+\pi^+\pi^-$.

The results include the first significant measurement of the total decay width of the D_{s1}^+. This width is determined to be

$$\Gamma(D_{s1}^+) = 0.92 \pm 0.03 \pm 0.04\,\mathrm{MeV},$$

compared to the 90% confidence level upper limit of 2.3 MeV given in Ref. [21]. The mass of the $D_{s1}(2536)^+$ is measured to be

$$m(D_{s1}^+) = 2535.08 \pm 0.01 \pm 0.15\,\mathrm{MeV}/c^2,$$

and the $D_{s1}^+ - D^{*+}$ mass difference to be

$$m(D_{s1}^+) - m(D^{*+}) = 524.83 \pm 0.01 \pm 0.04\,\mathrm{MeV}/c^2.$$

The result for the $D_{s1}^+ - D^{*+}$ mass difference represents a significant improvement compared to the current world average of $525.04 \pm 0.22\,\mathrm{MeV}/c^2$ [21].

Based on a decay angle analysis, the $J^P = 1^+$ assignment for the D_{s1}^+ meson is confirmed.

Acknowledgments

We are grateful for the extraordinary contributions of our PEP-II colleagues in achieving the excellent luminosity and machine conditions that have made this work possible. The success of this project also relies critically on the expertise and dedication of the computing organizations that support *BABAR*. The collaborating institutions wish to thank SLAC for its support and the kind hospitality extended to them. This work is supported by the US Department of Energy and National Science Foundation, the Natural Sciences and Engineering Research Council (Canada), the Commissariat à l'Energie Atomique and Institut National de Physique Nucléaire et de Physique des Particules (France), the Bundesministerium für Bildung und Forschung and Deutsche Forschungsgemeinschaft (Germany), the Istituto Nazionale di Fisica Nucleare (Italy), the Foundation for Fundamental Research on Matter (The Netherlands), the Research Council of Norway, the Ministry of Education and Science of the Russian Federation, Ministerio de Educación y Ciencia (Spain), and the Science and Technology Facilities Council (United Kingdom). Individuals have received support from the Marie-Curie IEF program (European Union) and the A. P. Sloan Foundation.

[1] B. Aubert *et al.* (*BABAR* Collaboration), Phys. Rev. Lett. **90**, 242001 (2003).
[2] B. Aubert *et al.* (*BABAR* Collaboration), Phys. Rev. Lett. **93**, 181801 (2004).
[3] V. Mikani *et al.* (Belle Collaboration), Phys. Rev. Lett. **92**, 012002 (2004).
[4] B. Aubert *et al.* (*BABAR* Collaboration), Phys. Rev. D **74**, 032007 (2006).
[5] D. Benson *et al.* (CLEO Collaboration), Phys. Rev. D **68**, 032002 (2003).
[6] P. Krokovny *et al.* (Belle Collaboration), Phys. Rev. Lett. **91**, 262002 (2003).
[7] R.N. Cahn and J.D. Jackson, Phys. Rev. D **68**, 037502 (2003).
[8] T. Barnes, F.E. Close, and H.J. Lipkin, Phys. Rev. D **68**, 054006 (2003).

TABLE IV: Summary of the systematic uncertainties for the mass difference ($\Delta_{\Delta m}$) and for the decay width (Δ_Γ).

	$\Delta_{\Delta m}$/ keV/c^2		Δ_Γ/ keV	
Systematic uncertainty	$K4\pi$	$K6\pi$	$K4\pi$	$K6\pi$
Resolution +10 %	< 0.5	< 0.5	±30	±30
MC validation	±7	±10	±1	±9
Alternative resolution models	< 0.5	< 0.5	±2	±12
Multi-Gaussian resolution: $r \pm \delta r$	< 0.5	< 0.5	±6	±7
Multi-Gaussian resolution: Parametrization of σ_0	< 0.5	< 0.5	±3	±2
Breit-Wigner signal line shape: Value of L	±9	±8	±2	±3
Mass window for $\Delta m(D_{s1}^+)$	< 0.5	< 0.5	±9	±3
Background parametrization	< 0.5	< 0.5	±5	±7
Tracking region material density	±21	±13	±14	±15
SVT Alignment	±6	±7	±2	±14
Magnetic field strength	±13	±19	±19	±11
Length scale	±4	±6	±8	±4
Drift chamber hits	±11	±15	±7	±7
ϕ-dependency	±13	±14	...	...

[9] W.A. Bardeen, E.J. Eichten, and C.T. Hill, Phys. Rev. D **68**, 054024 (2003).
[10] M.A. Nowak, M. Rho, and I. Zahed, Acta Phys. Polon. **B35**, 2377 (2004).
[11] E. van Beveren and G. Rupp, Phys. Rev. Lett. **91**, 012003 (2003).
[12] E.E. Kolomeitsev and M.F.M. Lutz, Phys. Lett. B **582**, 39 (2004).
[13] L. Maiani, F. Piccinini, A.D. Polosa, and V. Riquer, Phys. Rev. D **71**, 014028 (2005).
[14] K. Terasaki, Phys. Rev. D **68**, 011501 (2003).
[15] A. Dougall, R.D. Kenway, C.M. Maynard and C. McNeile (UKQCD Collaboration), Phys. Lett. B **569**, 41 (2003).
[16] G.S. Bali, Phys. Rev. D **68**, 071501 (2003).
[17] P. Colangelo, F. de Fazio, and R. Ferrandes, Mod. Phys. Lett. **A19**, 2083 (2004).
[18] E.S. Swanson, Phys. Rep. **429**, 243 (2006).
[19] The use of charge conjugated reactions is implied throughout the text.
[20] H. Albrecht *et al.* (ARGUS Collaboration), Phys. Lett. B **230**, 162 (1989).
[21] K. Nakamura *et al.* (Particle Data Group), J. Phys. **G37**, 075021 (2010).
[22] J. Alexander *et al.* (CLEO Collaboration), Phys. Lett. B **303**, 377 (1993).
[23] B. Aubert *et al.* (*BABAR* Collaboration), Phys. Rev. D **77**, 011102(R) (2008).
[24] V. Balagura *et al.* (Belle Collaboration), Phys. Rev. D **77**, 032001 (2008).
[25] B. Aubert *et al.* (*BABAR* Collaboration), Nucl. Instrum. Methods Phys. Res., Sect. A **479**, 1 (2002).
[26] D. Lange, Nucl. Instrum. Methods Phys. Res., Sect. A **462**, 152 (2001).
[27] S. Agostinelli *et al.* (GEANT4 Collaboration), Nucl. Instrum. Methods Phys. Res., Sect. A **506**, 250 (2003).
[28] F. von Hippel and C. Quigg, Phys. Rev. D **5**, 624 (1972).
[29] S. Chung, CERN Yellow Report 71-8 (1971).
[30] C. Amsler and C. Bizot, Comput. Phys. Commun. **30**, 21 (1983).
[31] J. Richman, CALT-68-1148 (1984).
[32] R.D. Field and S. Wolfram, Nucl. Phys. B **213**, 65 (1983).
[33] B. Aubert *et al.* (*BABAR* Collaboration), Phys. Rev. D **72**, 052006 (2005).
[34] L. Lyons, D. Gibaut, and P. Clifford, Nucl. Instrum. Methods Phys. Res., Sect. A **270**, 110 (1988).